RSC Advances

ROYAL SOCIETY OF CHEMISTRY

www.rsc.org/advances

Journal Name

ARTICLE

Selective 1,3-Butadiene hydrogenation by gold nanoparticles deposited&precipitated onto nano-carbon materials

E. Castillejos,[a*] B. Bachiller-Baeza,[b,c] E. Asedegbega-Nieto,[a] A. Guerrero-Ruiz,[a,b] and I. Rodríguez-Ramos,[b,c]

Abstract

Graphene oxide and multiwall carbon nanotubes (CNTs) were chemically modified by treatment with urea and subsequent annealing at different temperatures. These materials were used as supports for gold nanoparticles and the resulting samples have been applied as catalysts in the 1,3-butadiene partial hydrogenation reaction. Supports and catalysts were exhaustively characterized. It was shown that urea treatments modified the graphene surfaces and the morphology of CNTs, in both cases with incorporation of significant amounts of different nitrogen surface groups. The presence of these groups on few layered graphenes or on CNT surfaces modifies the gold precipitation-deposition process during catalysts preparation, giving place to different amounts of incorporated gold on the various supports. The obtained catalytic results suggested that the partial hydrogenation requires limited availability of hydrogen, and for this the migration through adsorbed species between metal and support to initiate the hydrogenation, probably by a spillover mechanism, seems to be a required step. In general intramolecular selectivity is structure-sensitive meanwhile catalytic activity is not structure-sensitive, as evidenced when the gold nanoparticle sizes are decreased.

[a.] Dpto. Química Inorgánica y Química Técnica, Facultad de Ciencias, UNED, Pº Senda del Rey 9, 28040 Madrid, Spain.
[b.] Unidad Asociada UNED-CSIC, Group of Design and Application of Heterogeneous Catalysts.
[c.] Instituto de Católisis y Petroleoquímica, CSIC, Cantoblanco, 28049 Madrid, Spain.

Introduction

Nowadays carbon nanostructures are one of the most commonly used materials in catalysis and have dominated some recent advances in nano-science and nano-technology. Carbon nanomaterials can be used either as supports for immobilizing active species or as metal-free catalysts [1]. Among the numerous carbon materials, graphite oxide (GO), graphene and carbon nanotubes (CNTs) exhibit many outstanding properties such as: large specific surface area, high electrical and thermal conductivity, chemical stability, high purity that eliminates self-poisoning, the possibility of tuning the specific metal–support interactions (which can directly affect the catalytic activity and selectivity) and the possibility of confinement effects in the inner cavity of CNTs or in the nanospace of the GO layers via intercalation [2-5].

One of the most developed methods to obtain GO is by strong oxidation of graphite [6]. After this initial oxidation step, and by means of mechanical/chemical or thermal exfoliation, it is possible to obtain graphene oxide sheets from GO. Finally, the eventual reduction of the graphene oxide sheets leads to graphene. Although the exact structure of GO is still subjected to intense debate, it is believed that the aromatic lattice of graphene is interrupted by epoxide entities, hydroxyl species usually placed in the interlayers and carboxylic groups that are located on the edges [7]. Hence, GO is a layered material with a high hydrophilic character and water molecules can readily intercalate between the layers. This results in an increase of the interlayer distance of GO as well as a change in hybridization of the oxidized carbon atoms from planar sp^2 to tetrahedral sp^3 [8]. Rapid heating of GO causes a rapid evaporation of the intercalated water, giving place to its expansion, reduction and delamination. Resulting graphene provides a two-dimensional model of catalytic support and it is one of the most promising materials in nanotechnology. Although the use of a single graphene sheet as catalytic support has not been reported, some promising results have already been obtained with materials containing few-layers of graphene [9]. On the other hand, CNTs may be viewed as a cylindrical structure formed from graphene sheets and closed or not by hemispherical caps at each end. They are hollow nanosized tubes and their nanometrical dimensions, together with the unique electronic structure of the graphene sheet, make the electronic properties of these one-dimensional structures highly unusual.

Several thermal and chemical processes can be used to tailor the carbon porous structure and the type and concentration of specific surface groups. A wide variety of oxidizing treatment techniques have been applied to functionalize the carbon surface: gaseous or liquid oxidizing

agents, chemical and electrochemical oxidations, plasma treatment, ion bombardment, etc [10]. Further modifications of carbon surfaces with other functionalities containing heteroatoms, like N and S, tend to increase their chemical reactivity and to give rise to building-blocks or starting materials for subsequent chemical modifications or applications, such as the anchoring of metal complexes to the support [11].

Gold nanoparticles attracted wide attention as catalysts only after the discovery that gold nanoclusters on oxide supports are highly active and selective, for instance, for oxidation reactions [11-15], hydrogenations [16,17], hydroaminations [18,19], organic reactions [20], and cross-coupling reactions [21]. Catalysis involving gold nanoparticles continues to show a fascinating future in this field and Au catalysts supported on Al_2O_3, SiO_2 or TiO_2 have shown special selectivity in catalysing the hydrogenation of 1,3-butadiene (BD) to butenes [22]. Purification of butane feed stocks that contain certain small amounts of butadiene is actually performed by selective hydrogenation of butadiene. A good process will consequently work in such a way that the partial hydrogenation of butadiene into butenes takes place, while avoiding any butane formation. Nanogold catalysts with selected supports like carbon materials can also promote high activity and high selectivity. In fact, so far there have been very few literature reports on the possible activity of Au-graphene or Au-CNTs. Chun Ming Xu et al [23] showed a striking enhancement of the catalytic performance of gold on CNTs for the hydrogenation of BD. However, since carbon materials are chemically inert, a pretreatment of the surface is needed for gold anchoring, involving oxidation of the surface by a strong oxidizing acid, or tedious metal catalyst synthetic procedures [24]. Deposition, adsorption, coprecipitación or use of monodispersed Au colloids are some of the most recent methods developed to deposit Au NPs. However in the case of the carbon materials none of these techniques are effective for depositing Au NPs. Theoretical studies have concluded that Au interactions with the graphite surface are weaker when compared to others supports [25].

Thus, to take advantage of all the potentiality of Au NPs supported on carbon materials, significant effort should be devoted to the synthesis of the catalysts, to the control of nanostructure morphologies and to their addressing. In this communication we report an efficient methodology to incorporate nitrogen on nano-carbon structures by thermal solid-state reaction between urea and nano-carbons (GOs, CNTs, etc.) and subsequent annealing at different temperatures. These nitrogen adatoms incorporated on the carbon nanostructures permit changes in the support properties. Thereafter, a deposition–precipitation synthetic procedure on

functionalized and nitrogen doped samples was used for the design of high-performance gold catalysts. Furthermore, we report the catalytic activity of Au NPs deposited on carbon structures for the selective hydrogenation of BD in H_2-rich streams. Characterizations of the carbon material supports and of the Au catalysts were performed using elemental analysis, nitrogen adsorption isotherms (BET), transmission electron microscopy (TEM), infrared spectroscopy, thermogravimetric (TGA), chemical titration and X-ray photoelectron spectroscopy (XPS). The synthesis of catalysts, relative catalytic activity of the materials and some structure-property correlations, are presented, focusing on the influence of the size of the gold NPs on the catalytic activity and selectivities as well as in the influence of the different supports.

Experimental

Synthesis of nano-carbon materials

Three types of nano-carbon materials were used in this study: graphite oxide (GO), commercial CNTs (CNT) and nitrogen-doped CNTs (CNT_N) prepared in our laboratory. GO was synthesized from natural graphite powder (99.999 % stated purity, 200 mesh) following a modification of the Brodie's method [26,30]. Briefly the graphite was added to a reaction flask containing fuming HNO_3 (20 mL/g of support), which was previously cooled to 0 ºC in an iced bath, after that potassium chlorate (8 g/g of support) was slowly added. The reaction was left to proceed for 21 h under stirring, and the final solid was filtered, extensively washed with deionized water until neutral pH, and dried under vacuum at 323 K overnight. CNT_s were obtained from Nanocyl^{TM}, 3100 Series, 95% purity. These CNTs were further oxidised by nitric acid at 120 ºC for 8h. For comparison another aliquot of these CNTs were also oxidized at 120 ºC for 24h (CNTox). Nitrogen-doped nanotubes CNT_N have been produced by catalytic chemical vapor deposition in a fluidized bed reactor on Fe/SiO_2 catalysts from acetylene-ammonia mixtures at 1023 K [29]. These CNT_N were characterized in our previous works and they presented a bamboo-like structure with graphene layers perpendicular to the CNT axis [11,29].

Preparation of urea modified supports

These support materials were prepared following a thermal solid-state reaction method, similar to that described by Z. Mou et al [27]. In this synthesis, GO (with an oxygen content about 25%)

was finely ground together with urea in the ratio of 1:3. The resulting mixture was introduced in a ceramic boat and placed in the middle of a quartz tube within a horizontal furnace. The sample was heated under nitrogen flow (100 mL/min) at a rate of 1°C/min until 180°C and thereafter at 5°C/min up to the desired temperature and then maintained at this temperature during 2 h. Three different temperatures were studied: 300, 450 and 600°C. Thereafter, samples were cooled down to room temperature under an inert nitrogen atmosphere and washed in hot water thoroughly until all unreacted urea was eliminated. The samples were labelled GO_{300}, GO_{450} and GO_{600} respectively. The same procedure was carried out for the synthesis of CNT_{300}, CNT_{450} and CNT_{600} supports, but in this case oxidized CNT was employed instead of GO.

Preparation of supported gold catalysts

Deposition-precipitation method was used in order to synthesize the gold catalysts. A solution of [$HAuCl_4$] in a mixture water/methanol (15/1) was added to the selected carbon support. After ultrasonic treatment at 283 K for 5 minutes, it was treated with a water solution of NaOH (0.2 M) until pH = 11. Then, the precipitate was stirred in an iced bath for 5 h and collected by filtration. Finally, the precipitate was washed with deionized hot water, until no Cl⁻ was detected. The sample was dried overnight at 373 K in air. The corresponding catalysts were labelled $AuGO_{300}$, $AuGO_{450}$, $AuGO_{600}$, $AuCNT_{300}$, $AuCNT_{450}$ $AuCNT_{600}$ and $AuCNT_{N}$. These samples were subjected to a pretreatement in flowing N_2 at 300°C for 1 h previous to the hydrogenation reaction tests. The following scheme (Scheme 1) summarizes the experimental procedure for the preparation of the catalytic systems.
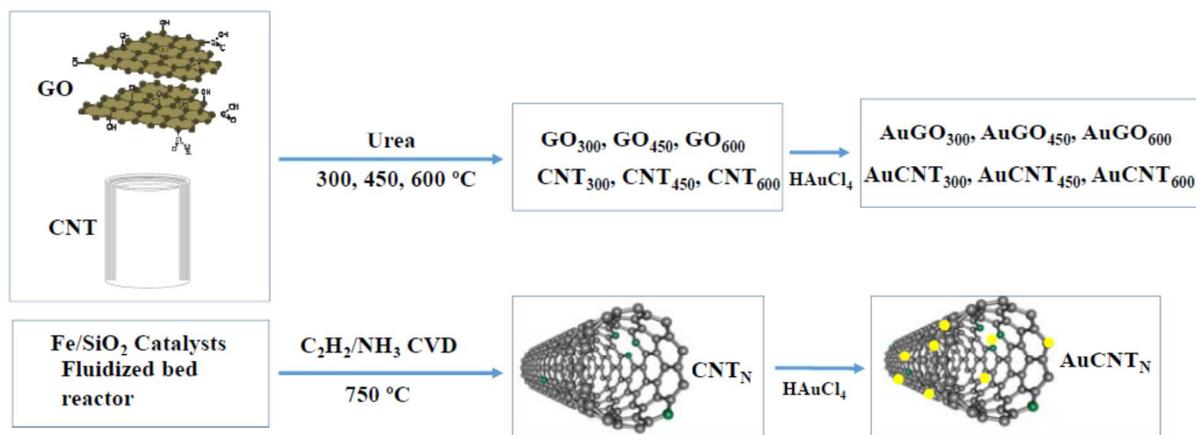
Scheme 1. Procedure for catalysts preparation

Instrumentation and Measurements

The BET surface area of the supports was measured from the nitrogen adsorption isotherm on an ASAP instrument. All the samples were characterized by X-ray photoelectron spectroscopy (XPS), thermogravimetric analyses and transmission electron microscopy (TEM). XPS analysis was performed with an ESCA-PROBE P (Omicron) spectrometer by using non monochromatized Mg-K radiation (1253.6 eV). Thermogravimetric analyses (TGA) were conducted under nitrogen in a TA instruments, model SDT Q600 TA System. The sample ($\sim$ 5 mg) was placed in a platinum crucible and heated with a $10°C.min^{-1}$ ramp between 298 and 1273 K, followed by an isotherm at that temperature for 30 minutes. TEM micrographs were performed on a JEOL JEM-2100F microscope at 200 kV. The average metal particle sizes were calculated using the following formula: $d_{Au} = \sum n_i d_i / \sum n_i$.

The chemical nature of the surface functional groups was evaluated by temperature programmed desorption coupled with mass spectrometer (TPD-MS). These experiments were performed under vacuum in a conventional volumetric apparatus connected to a RGA-200 SRS mass spectrometer [28]. The sample was evacuated for 30 min at room temperature and then ramped to 1023 K at a 10 K min^{-1} rate. Considering that the gases evolved during the TGA experiment are CO_2 and CO, as it is evidenced from the TPD-MS, and that the range of temperatures at which the evolution takes place is different; the amount of carboxyl can be estimated by the weight loss up to 723 K, while phenol–carbonyl groups correspond to the mass loss from 723 K up to 1100 K. Infrared (KBr pellets) spectra were obtained on a FT-IR (Varian 670) spectrometer. Finally X-ray diffraction (XRD) patterns were obtained on a Polycristal X'Pert Pro PAnalytical diffractometer with Ni-filtered Cu/Kα radiation (λ= 0.1544 nm) operating at 45 kV and 40 mA. For each sample, Bragg's angles between 4° and 90° were scanned at a rate of 0,04 deg/sec. The gold content in the catalyst was determined by acid digestion of the catalyst followed by ICP-OES analysis.

The catalytic experiments for BD hydrogenation were carried out in a continuous flow fixed-bed reactor. The mixture of reactants, H_2 (10% vol) and BD (2 % vol) in N_2 passed through the catalyst bed a rate of 60 mL/min. The hydrogen amount was in large excess. The reaction temperature was varied between 70 and 200 ºC at atmospheric pressure. Before reaction, the catalyst was pretreated in flowing N_2 at 300 ºC for 1 h. The reactor effluent was online analyzed

using a gas chromatograph with flame ion detector (FID) and thermal conductivity detector (TCD) with a 20% BMEA Chromosorb P80/100 column. The catalyst activity was calculated as:

$$(((\frac{CBD_i - CBDf}{BD_i})/gAu) \; x \; 100\%,$$

Where CBD_i represents the initial BD molar flow rate (mmol/min) and CBD_f the final BD molar flow rate. The selectivity of each product was calculated as;

$$\frac{C_P}{C_T}x \; 100\%,$$

Where C_P represents the molar flow rate of the product whose selectivity is being calculated and C_T represents the total molar flow rate of all the products.

Results and discussion

Characterization of carbon materials

Graphite oxide and CNTs were modified by a thermal solid-state method with urea and annealing at different temperatures, i.e. 300, 450 and 600 °C, in order to yield different amounts of nitrogen surface groups. BET surface areas calculated from N_2 adsorption isotherms (type IV isotherms were observed) gave values ranging from 20 up to 30 m^2/g for the modified graphene oxide samples and from 200 up to 300 m^2/g for the modified CNTs. Figure 1 shows TEM micrographs of the GO_{450} and CNT_{450} after annealing as representative of the modified supports.
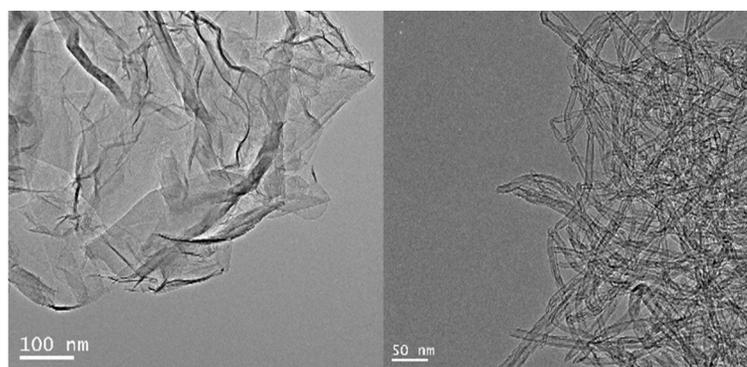

Figure 1. TEM micrographs

The nature and concentration of the nitrogen surface groups produced by this preparation method was determined by elemental analysis and surface semi-quantitative analysis (XPS). These results are shown in Table 1. After annealing, the N content determined by elemental analysis was

between 26.7-19.5 wt.% for the GO_{300}, GO_{450} andGO_{600}; while for CNT_{300}, CNT_{450} and CNT_{600} diminished from 5.6 to 3.1 wt.%. Such values were close to those obtained by XPS. Hence, it was proven and confirmed that thermal solid-state reaction with urea carried out at different annealing temperature is an effective method to produce N-doped carbon materials. On the other hand, the maximum N content corresponds to GO_{300}. A decrease in N content was observed when increasing the annealing temperature, both for the GO_{series} and CNT_{series}. These results seem to indicate that the incorporation of nitrogen species takes place at low temperatures, probably near the melting point of urea (133ºC). In the case of the graphite oxide this reaction gave rise to graphene surfaces, which have high amount of N-doping adatoms. Also, it appeared that when heating these N-doped graphenes at higher temperatures, a fraction of the nitrogen functional groups is slowly released. The incorporation of nitrogen atoms in CNTs was lower than for GO series, pointing to a lower reactivity. Finally, for comparative purposes we have studied a CNT_N sample, which was grown in a fluidized bed reactor using an ammonia/acetylene reaction mixture over a Fe/SiO_2 catalyst [29]. The reported data in Table 1 reveal that nitrogen incorporated for this sample was lower in comparison with CNT series and corresponds to our previous published data [11].

Table 1. Elemental and XPS analyses of GO_{series}, CNT_{series} and CNT_N

	XPS (Mass %)			Elemental analysis (wt. %)		
	C	O	N	C	O	N
GO_{300}	57.0	16.5	26.5	49.1	22.2	26.7
GO_{450}	78.7	2.3	16.8	69.1	8.7	21.1
GO_{600}	89.3	0.9	8.5	79.0	1.0	19.5
CNT_{300}	85.6	5.1	9.8	86.7	7.0	5.6
CNT_{450}	94.0	2.0	4.0	85.9	8.6	4.9
CNT_{600}	92.4	3.5	4.0	88.6	8.0	3.1
CNT_N	88.7	7.1	4.2	89.5	5.8	2.6

Figure 2 shows the XRD diffractograms for all the modified supports (GO_{series} and CNT_{series}). XRD is an effective method to study the interlayer changes of graphite related materials. GO had a characteristic peak at $2\theta=16º$ [30]. This peak disappears after the functionalization treatment, and another peak at 26.5º, corresponding to the graphite diffraction (002) peak, becomes relevant. This confirms the presence of graphitic ordering due to reduction during urea treatment. When the annealing temperature increases, the (002) peak intensity decreases significantly, suggesting the

presence of exfoliated graphene oxide. In addition, for GO_{300}, there are some peaks attributable to cyanuric acid. This latter compound could be produced during the reduction reaction of GO with urea and/or could be originated by the progressive degradation of the initially produced nitrogen surface groups. Here it is important to notice that ammonia gas was also released during the annealing reaction as a consequence of the thermal decomposition of urea.

The XRD diffractograms of CNTs show the typical peak at 2θ=25° assigned to the CNT 002 plane, that is graphite peak slowly shifted. The peak intensity of (002) for CNT_{300} sample is smaller, indicating a diminished crystallinity of these nanotubes, which could be assigned to the presence of the nitrogen species produced from the reaction with urea.
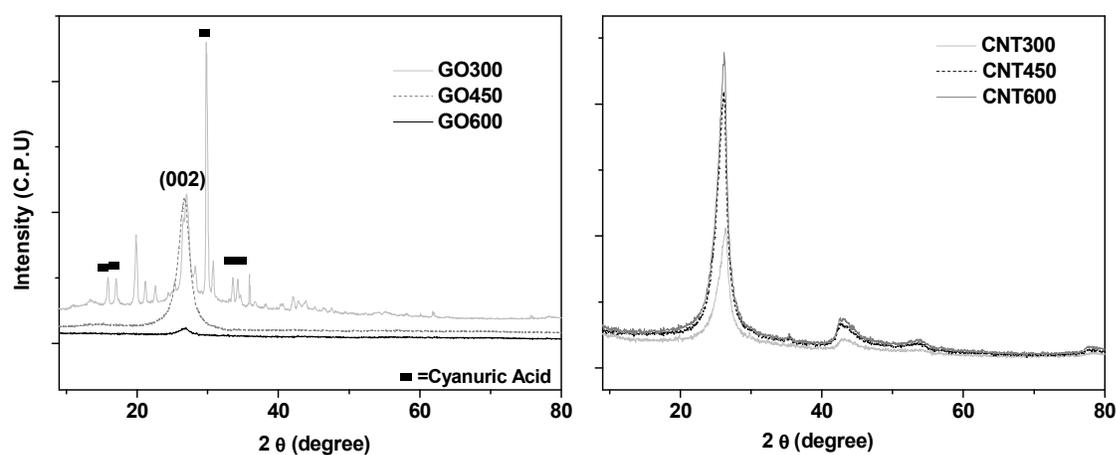

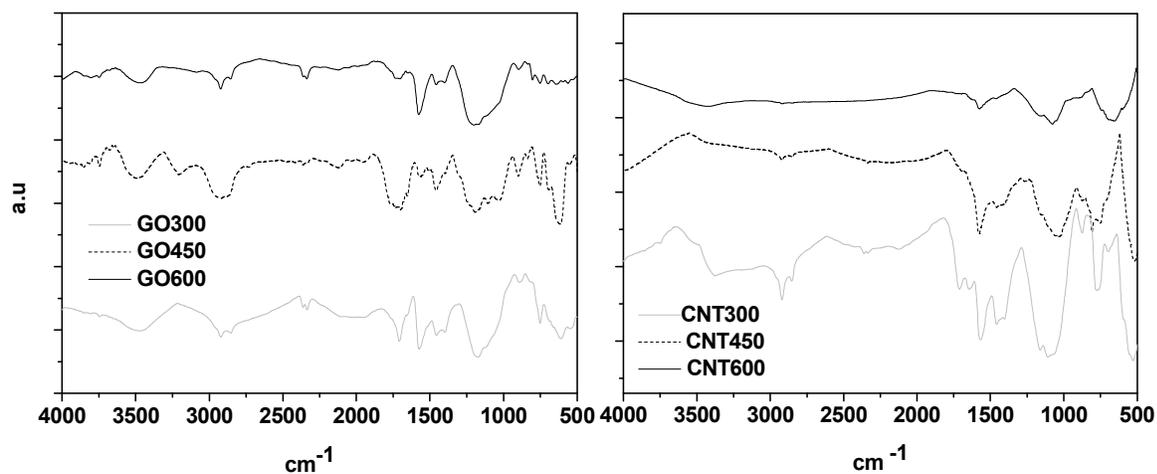Figure 2. XRD of GO_{series} and CNT_{series}: (■= Cyanuric acid diffraction peaks)

Figure 3. Infrared (KBr pellets) spectra of GO_{series} and CNT_{series}

Figure 3 shows the infrared spectra of all the samples. In the spectrum of the modified GO, the peaks at 3005 and 1580 cm^{-1} are characteristic bands of C–H and C=C stretching of the aromatic ring. Peaks at around 1579 and 1466 cm^{-1} could be due to C=N stretching and -NH$_2$ bending, respectively. This could be an indication of the presence of melamine [31] or pyrrolic and pyridinic groups [32]. There is a collection of overlapping bands in the 1000–1300 cm^{-1} range. They correspond to C-N stretching of incorporated nitrogen or C-O-C groups of the non-fully reduced GO. This later would be more likely present in the samples treated at lower temperature which still partly retain some of the original GO oxygenated groups. The FT-IR spectrum of GO$_{450}$ differs from that of GO$_{300}$ as evidenced by the presence of new peaks at 3252 and 1650 cm^{-1} as it can be clearly seen in Fig. 3. These peaks were assigned to N–H stretching and C=O stretching of amide groups [33] on the GO$_{450}$ surface, respectively. These results clearly indicate the formation process of N-doped graphene below 450º via amide linkages between the ammonia produced by decomposition of urea and the oxygen functional groups of the graphene sheets. Finally, the FT-IR of GO$_{600}$ does not show amide peaks. In this case, the amide groups were transformed to pyrrolic and pyridinic groups at the graphene edges and/or defect sites, and to "graphitic" N in the graphene network. These features are also obvious for the CNT samples.

Furthermore, thermogravimetric analyses under nitrogen (Fig. 4) show that the decomposition manner was different for each sample indicating that the presence and nature of the formed nitrogen surface groups strongly depend on the temperature of the urea reduction treatment. GO$_{300}$ decomposition started at about 300 ºC and the total mass loss was 46%. Desorption of nitrogen surface groups can also be followed on viewing the derivative weight loss where various maxima are observed. These peaks are clearly not the same for the other two GO urea-treated samples. The higher the treatment temperature, the lower the weight loss and the higher the decomposition temperature. The CNT series showed a similar tendency (Fig. 4), although the weight loss for GO samples was much higher due to the higher amount of nitrogen groups formed during the urea treatment.
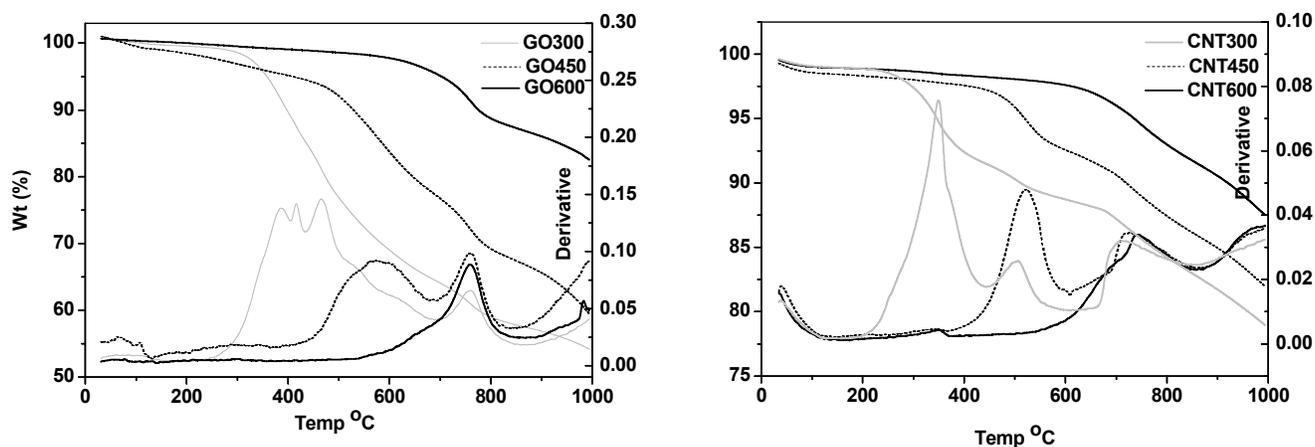
Figure 4. TGA under nitrogen of GO_{series} and CNT_{series}

The chemical nature of the surface functional groups was also evaluated by temperature programmed desorption coupled with mass spectrometry (TPD-MS). The observed profiles are displayed in Figure 5. The molecular ion of urea (m/z=60) was not detected in any case. The presence of m/z=43 ion (considered to be isocyanic acid), m/z=27 (hydrogen cyanide) and m/z=17 (ammonia) during decomposition of GO_{300} sample revealed a large variety of nitrogen surface groups in this material [34-36], which in part could be assigned to strongly adsorbed quasi-urea species. The simultaneous detection of m/z=44 signal (carbon dioxide) and m/z=17 (ammonia) could be consequence of a reaction among the isocyanic acid evolved and residual water molecules. Notice that the isocyanic acid only appeared on the GO_{300} sample. In the case of the sample prepared by annealing at 450 ºC (GO_{450}), the main observed fragments are those of masses (m/z) 17, 16, 44, 27 and 28, which could correspond to the decomposition of N-amide linkages with the oxygen functional groups of the graphene sheets reacted up to 450ºC [37,38].

Finally, for GO_{600} sample only fragments evolved at higher temperatures were observed. In this case, it is possible that the nitrogen atoms could have been incorporated into the graphite layers replacing carbon atoms. In short the TPD-MS experiments reveal a remarkable variety in the nature of the nitrogen species generated on the GO when reacted with urea. Also the stability of each species depended on the temperature applied during the annealing preparation procedure. Most of these species were also detectable in the TPD experiments of urea treated CNT supports although there are some significant differences (Fig. 5). While in GO_{300}, m/z= 44 (CO_2) is by far the most intense signal, in CNT_{300} sample it is largely reduced when compared to other species present whereas the relative intensity of m/z=43 (isocianic acid) has greatly increased. This is an

indication that the nature of products formed during urea thermal treatment depended also on the characteristics of the carbon materials.
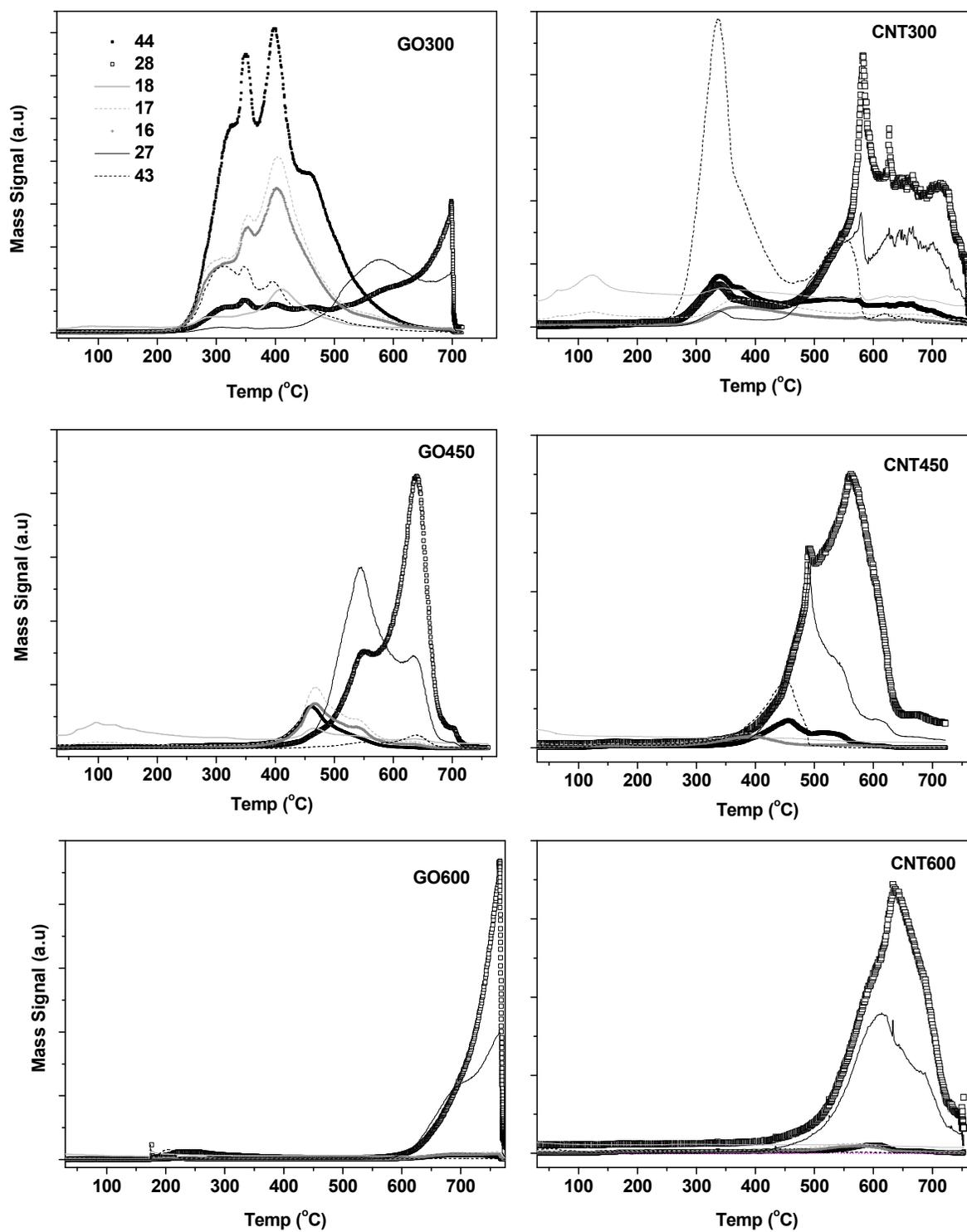
Figure 5. TPD profiles of GO_{series} and CNT_{series}

The qualitative results obtained from TPD-MS were further checked by a surface analysis of these materials, so they were also studied by XPS. As already mentioned, Table 1 summarized the mass percentages of elements present in each sample. The GO employed as starting material exhibits higher oxygen content (25%) and during treatment with urea this content was reduced at expense of the formation of nitrogen surface groups. N and O content are highest for GO_{300} when compared with the other two urea-treated samples obtained at higher reaction temperatures. This is due to the GO reduction process as well as to the evolution of different nitrogen-containing compounds when heating at higher temperatures. This can be better understood on viewing the envelope of C 1s XPS peak of the urea-treated materials (Fig. 6 a). The physical mixture of urea and GO (without undergoing any thermal treatment) was also included and serves as comparative reference. Three maxima can be deduced from this last mentioned physical mixture sample (Fig. 6 a). First two owing to C-C (at 284.6 eV) and C-O (at 286.6 eV) species characteristic of GO materials [39], and the third at about 288.8 eV owing to the amide groups of urea. When this physical mixture was treated under nitrogen at 300 ºC yielding GO_{300} sample, the second maximum, at 286.6 eV, drastically reduces owing to the diminution of epoxide groups occurring in the reduction process of GO. At the same time, the maximum for amide groups observed in the physical mixture has been shifted to higher binding energies, becoming quite large and much wider. Thus, it could be deconvoluted in several peaks, due to the presence of various species that as observed in TPD-MS experiments gave different thermal decomposition products. When treatment temperature was increased to 450 ºC, this peak is significantly reduced and shifted to lower binding energy values (287.8 eV). This is due to transformation of initial amide species into other ones, and from these XPS spectra can be ascribed to –N-C=O species [40]. As for the GO_{600} sample the peak, although greatly reduced, is still present.

Further details on the surface groups formed during urea treatment can be obtained from the inspection of N 1s XPS spectra represented in Fig. 6 b. While the N 1s peak recorded for untreated urea appears at a binding energy of 398.7 eV, the N 1s envelope obtained for GO_{300} sample is larger and wider and could be deconvoluted into three different species. This is in agreement with the results observed in C 1s XPS data. These three contributions to the N 1s peak are centered at about, 398.3, 399.8 and 401.5 eV and could be ascribed to triazine groups (C=N-C) and –NH groups [41]. These data indicate the possible formation of ammelide and/or

melamine intermediates during the urea treatment, as well as some alternative species of the type protonated amides or pyridine groups [42]. As for GO treated with urea at 450 ºC, three N regions appear (Fig 6 b). Lowest binding energies of about 398 eV can be ascribed to pyridinic nitrogen, the middle region whose value is 399 eV normally refers to pyrrolic nitrogen, amides or amines, while at 401 eV we have quaternary nitrogen [43-45]. This last species increases at the expense of the middle region as annealing temperature was increased from 450 to 600 ºC.

Massive % of C, O and N for the urea CNTs treated samples obtained from XPS analysis, were also collected in Table 1. The low oxygen content (2.8 %) of the original CNT sample obtained after oxidation treatment points to a CNTs low reactivity. Although nitrogen incorporation was significantly lower in all cases, the tendency observed on increasing temperature treatment was similar to that observed in GO supports. Fig. 6 c, illustrates the C 1s envelopes for the three temperature urea-treated CNTs where a small hump is only apparent for the CNT_{300}. Fig. 6 d also shows the N 1s spectra of the studied CNT supports. For CNT_{300} the N 1s spectra can be deconvoluted in two contributions (at 398.9 and 400.2 eV) due to the presence of urea decomposition products. Increasing the treatment temperature gives rise to the appearance of pyridinic, pyrrolic/amide and quaternary nitrogen. At higher temperature (600 ºC) there is an increase in the quaternary nitrogen and a decrease in the pyrrolic/amide nitrogen groups. This is in agreement with literature findings were studies involving stability of nitrogen surface groups on CNTs indicated that at higher temperatures the main species present were pyridinic and quaternary nitrogen [38]. This is similar to what was observed for GO samples.

A new sample of CNTs containing a higher number of oxygen groups (CNT_{ox}) was selected for comparison and was also treated with urea at 450 ºC. The presence of higher oxygen quantity was confirmed by XPS (10.3%) and for the sake of brevity their XPS envelopes are not included. Annealing of this urea-treated CNTox at 450 °C did not produce a significant change in the nitrogen surface group concentration when compared to the initial CNT_{450}. Hence, the formation of nitrogen groups is independent of the concentration of oxygen groups on the surface.

In the case of the CNT_N sample, where ammonia was used in the preparation procedure [29], three of the earlier mentioned peak contributions were found, and assigned to pyridinic, pyrrolic and quaternary nitrogen species (Fig. 6 d). The ratio of the last to the first was much higher than what has been observed for all other samples while the pyrrolic nitrogen is almost absent. Moreover a small peak at higher binding energy due to NO groups (405 eV) was present [29].
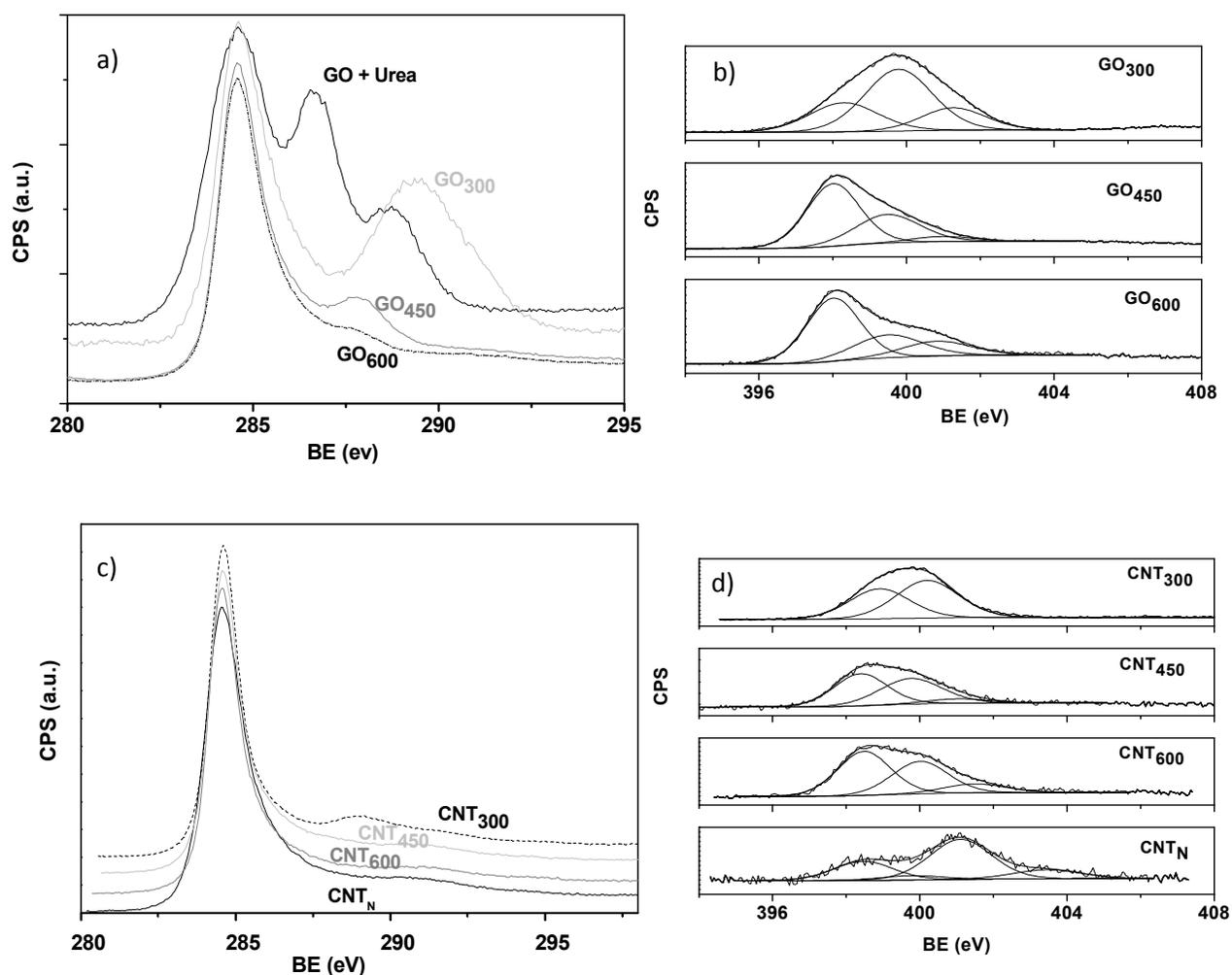
Figure 6. XPS spectra of: a) C 1s GO$_{series}$, b) N 1s GO$_{series}$, c) C 1s CNT$_{series}$ and d) N 1s CNT$_{series}$

This systematic study of the samples treated by thermal annealing has shown the incorporation of nitrogen atoms into the graphene or CNT structures, and/or the formation of amide groups, which were anchored over initially presented oxygen functional groups. These carbon materials contain nitrogen in different forms including pyridinic, pyrrolic and quaternary species. Doped nitrogen CNT$_N$ also contains nitrogen in different forms though the XPS spectrum, is somewhat different mainly presenting pyridinic and quaternary nitrogen species while the pyrrolic nitrogen is almost absent. The N incorporates one more electron into the structure of carbon surface and then the

carbon surface will become more basic in character which improves the electronic density. Therefore, p electron delocalization will occur easily owing to their structure, and the electron donor effect of N can also make the bonding stronger. The basicity of GO_{450}, GO_{600}, CNT_{450}, CNT_{600} and CNT_N samples after treatments will allow deposition-precipitation of gold on these surfaces where it is indeed complicated [22]. In general, carbon has found limited use as Au support in hydrogenation reactions due to the difficulty in obtaining a well-dispersed Au phase with a narrow size distribution [46]. Therefore, urea and ammonia treatments can be used to change the carbon properties and provide a suitable surface for attaching Au NPs.

Characterization of the supported catalysts

Chemical analyses of the gold precursor anchored on the surface of graphene and CNTs (Table 2) allowed us to know the Au loading for the GO_{series}, CNT_{series} and CNT_N surfaces. Exhaustive characterization indicated this gold was presented in the form of NPs associated to the graphene sheets or CNTs. The XRD difractograms of AuGO and AuCNTs (Fig. 7) showed typical peaks at 2θ=26.5º (discussed above) and the peaks at 2θ values of 38.4º, 44.6º, 64.8º that were assigned to gold. The average particle size of the supported Au on GO_{series} and CNT_{series} was determined with the Scherrer equation using the Au (111) reflection as reference for the peak broadening analysis (Table 2). As a result, $AuGO_{450}$ showed a particle size of 19.0 nm and $AuGO_{600}$ gave values of 33.5 nm. On the other hand, $AuCNT_{450}$ showed a particle size of 16.7 nm and $AuCNT_{600}$ of 23.8 nm. Finally $AuCNT_N$ yielded an average particle size of 13.7 nm. The Au NPs average particle sizes increased for the supports treated at higher annealing temperatures. Although the reasons for these NP sizes were not clear, one could speculate that higher NP dispersions could be related to a higher content of nitrogen groups on the surface. For the GO_{series}, the intensity of (002) peak decreases in the order GO_{300}>GO_{450}>GO_{600} indicating the presence of expanded graphene oxide in the samples annealed at higher temperatures. $AuGO_{300}$ exhibits a small peak at 13.4º that may be due to the existence of graphene oxide which comes from the incomplete reduction of graphite oxide during the annealing process or the presences of other species introduced during this process. $AuGO_{300}$ does not have Au NPs since GO_{300} presents a low isoelectric point (below 5) and thus at higher pH the surface will be negatively charged, resulting in an electrostatic repulsion of gold-containing anions. Therefore, Au precipitates only in the liquid phase and not over the support surface [22]. This feature is also obvious for CNT_{300} sample. That means that GO_{300} and CNT_{300} are not suitable to prepare Au NPs supported catalysts.

Table 2. Gold loading and average particle size determined by TEM and XRD.

Catalyst	Au NP size (nm)		(wt. %)[a]
	TEM	XRD	
AuGO$_{450}$	16.6	19.0	2.8
AuGO$_{600}$	18.9	33.5	2.9
AuCNT$_{450}$	30.0	16.7	2.7
AuCNT$_{600}$	29.0	23.8	3.7
AuCNT$_{N}$	12.7	13.7	3.6

[a]Determined by ICP-MS.
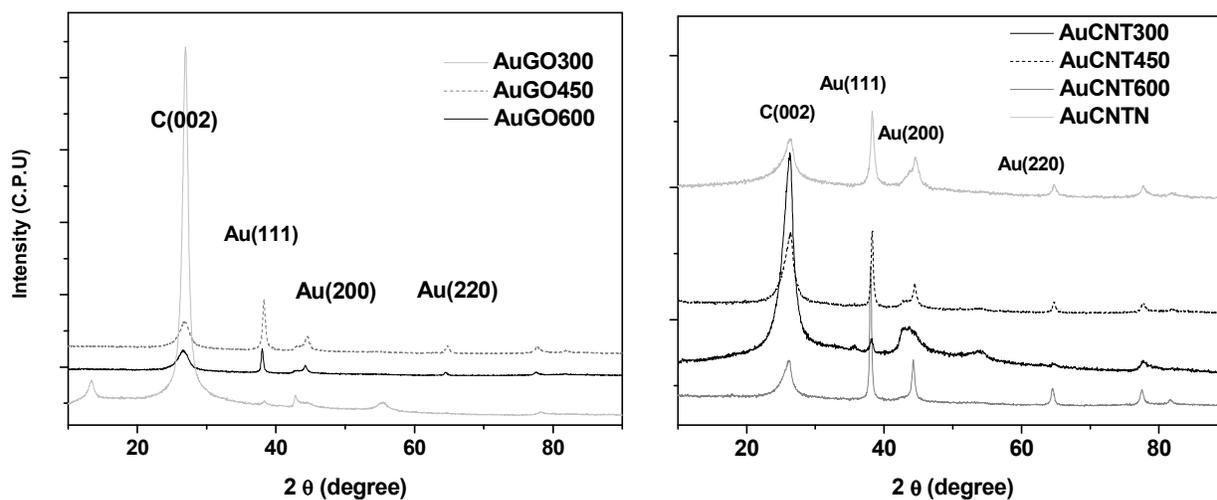
Figure 7. XRD of AuGO$_{series}$ and AuCNT$_{series}$

Figures 8 and 9 show representative TEM micrographs and AuNPs size distributions of the different GO decorated with Au NPs and of the AuCNT$_{N}$ sample, respectively. In general TEM images of the GO supports revealed the presence of packs of flat graphitic layers with different sizes and wrinkled sheets. Moreover, these samples were composed of different number of stacked graphene layers depending on the temperature of the annealing process. Comparing the TEM images and XRD profiles for each sample, it seems that a reasonably efficient GO reduction was attained, especially for AuGO$_{600}$ where most of the sheets are delaminated. The Au NPs average diameter obtained by TEM for the ex-GO supported catalysts are summarised in Table 2.

On the other hand, $AuCNT_N$ yielded the smallest particle size by both XRD and TEM. In the case of $AuCNT_{450}$ and $AuCNT_{600}$ catalysts the TEM determined average Au particle sizes are close to 30 nm. In general, it has been observed for all samples that the Au particles were not homogeneous in size. Furthermore, even though the mean particle size was quite large, samples contain a significant population of small Au NPs that should be taken into account when interpreting the catalytic results.
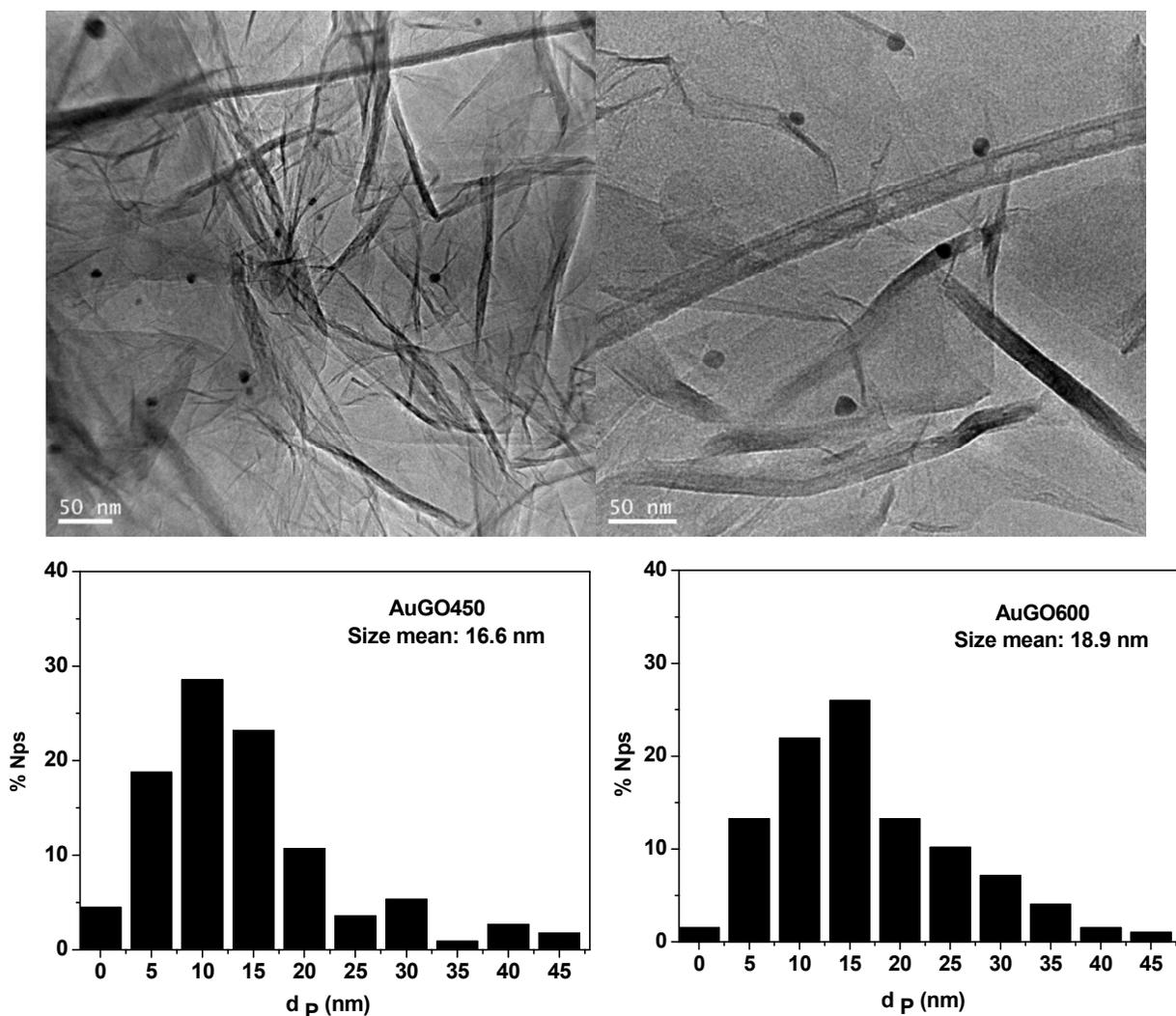

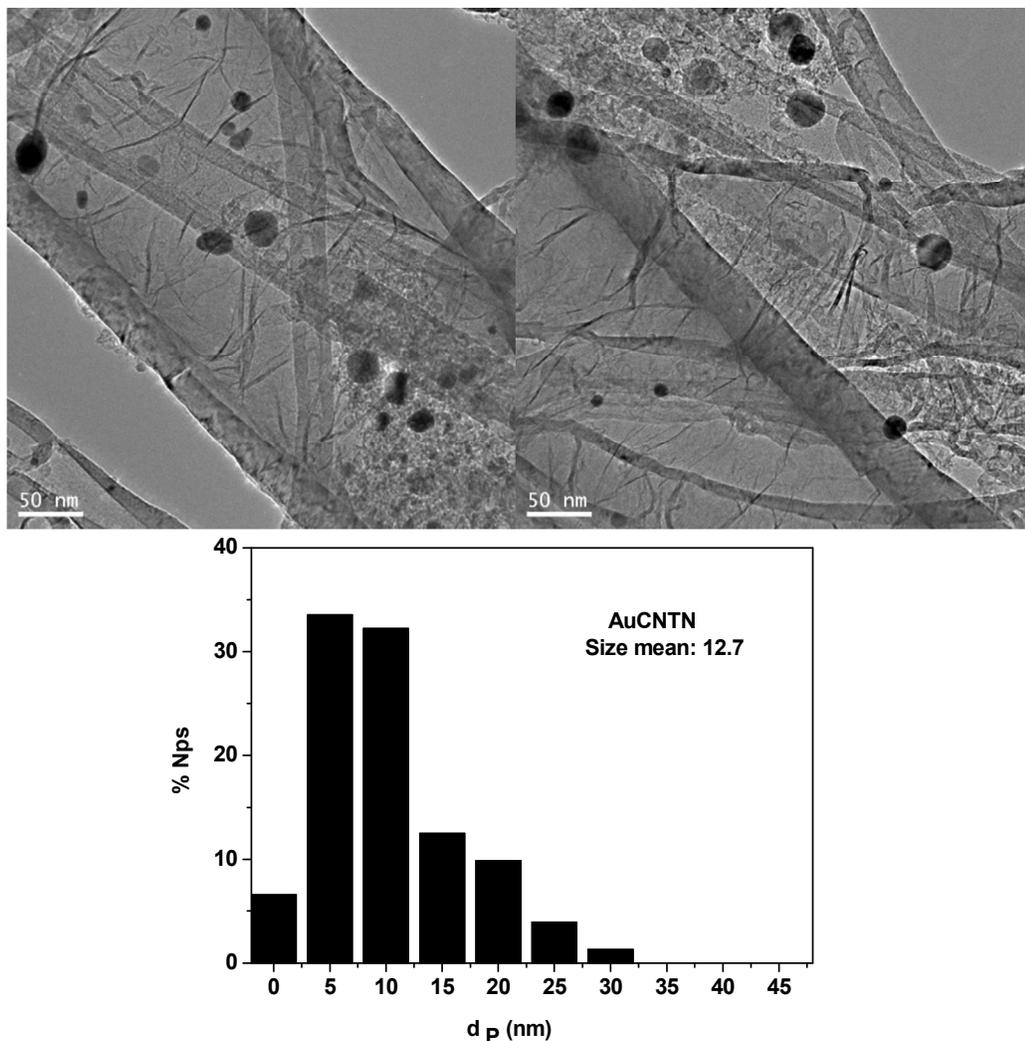Figure 8. TEM micrographs and histograms with the size distribution of $AuGO_{450}$ and $AuGO_{600}$.

Figure 9**.** TEM micrograph and histogram with the size distribution of AuCNT$_N$

Figure 10 represents the XPS Au 4f$_{7/2, \, 5/2}$ doublet spectra of the catalysts with binding energies in the range 84.2-87.8 eV. These were typical values for Au (0) [14], indicating the formation of metallic Au NPs on the supports. XPS envelop can be deconvoluted into more than one peak bearing in mind the presence of different Au species of varying particle size. A detailed study involving size dependent XPS spectra on Au nanoclusters proved that binding energy varies with particle size [47]. Other authors such as Mikhlin et al [48] also claimed that increase in binding energy of less than 1 eV with respect to that of the bulk metal can be attributed to Au^0 NPs. Taking this into consideration, in our study the Au was fitted to two peaks. The component at a binding energy approaching 84.0 eV could be assigned to metallic gold larger than 5 nm while

values of about 0.7 eV higher were ascribed to sizes below 5 nm. The Au 4f binding were listed in Table 3. Figure 10 show changes regarding Au NPs binding energy on CNT_{450}, GO_{450} and GO_{600} shifting to higher BE when compared to CNT_{600} and $AuCNT_N$. This is probably due to different Au-support interactions and one can speculate that it could be related to the support surface composition.

The Au NPs species percentages were determined by XPS and compared to TEM distribution. As can be observed, the concentration of Au NPs estimated by XPS (Table 3) and by TEM (Fig. 8 and 9) are significantly different. In the first case, the proportion of NPs < 5nm (obtained by XPS) are higher than those determined by TEM. This suggests that the Au NPs < 5nm are located directly on the catalyst surface and the NPs > 5 nm, due to its greater depth are not fully penetrated by this X-ray source. Hence, are out of view of the XPS analysis. It should be noted that TEM analysis have a much higher resolution when compared to XPS analysis. In general Au NPs on CNT_{600} and CNT_{450} show lower proportion of NPs < 5nm when compared to the other samples studied.
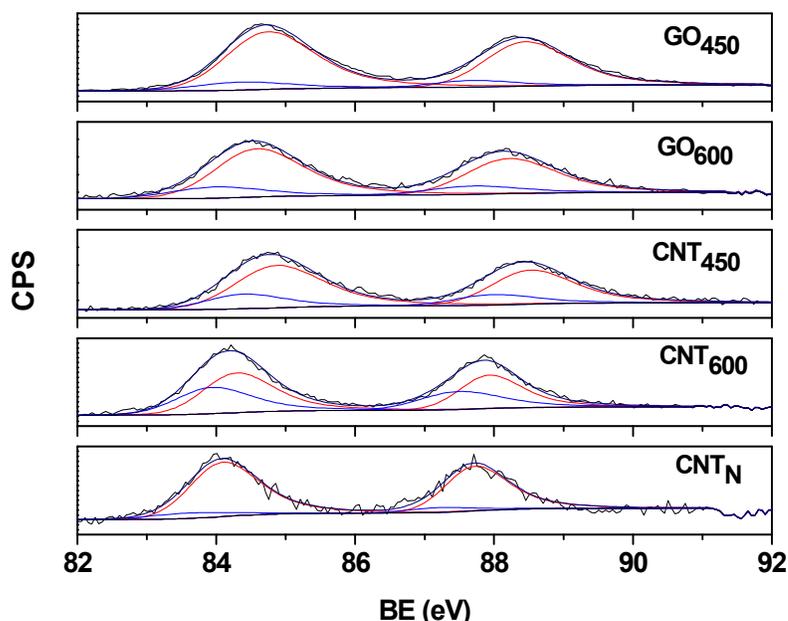

Figure 10. XPS spectra deconvolution of the $AuGO_{series}$, $AuCNT_{series}$ and $AuCNT_N$

Table 3. Au $4f_{7/2}$ binding energy (BE) and atomic % of NPs

	Au°NPs(<5mn)	Au°NPs(>5nm)
AuGO$_{450}$	84.8 (87.1%)	84.3 (12.9%)
AuGO$_{600}$	84.6 (80.2%)	84.0 (19.8%)
AuCNT$_{450}$	84.9 (76.3%)	84.4 (23.7%)
AuCNT$_{600}$	84.3 (58.6%)	83.9 (41.4%)
AuCNT$_{N}$	84.1 (89.7%)	83.6 (10.3%)

The present results showed that nitrogen-doped GOs and CNTs have an interesting potential for the incorporation of Au NPs by the deposition-precipitation method, but this simple method can only be applied when the supports have an isoelectric point above 5 [49] and is not effective for depositing Au NPs on GO$_{300}$ and CNT$_{300}$ materials. The highest PZC of nitrogen-doped carbon materials (PZC~7) compared to many carbon materials (PZC~4) may favour the restraining of the Au species. This fact can explain the relatively large Au nanoparticles obtained with our supports. On the other hand, Dommele et al [50] demonstrated that nitrogen-containing CNTs display basic properties, and had established that N must play an essential role in the deposition of Au NPs.

Catalytic Results

Butadiene hydrogenation is a consecutive reaction that according to reaction conditions (temperature, butadiene and hydrogen ratio, etc) can show very different behaviour in terms of conversion and selectivity to butenes (selective hydrogenation) or butane (unselective total hydrogenation). When the reaction parameters are kept constant, BD hydrogenation can be considered a typical surface sensitive reaction and the conversion and selectivity to butenes can mainly be related to Au NPs morphology or size. However, some studies have shown that BD hydrogenation over Au catalysts was somewhat insensitive to the Au particle size and composition of support [51]. In general, the low catalytic activity of Au catalysts in hydrogenation has been attributed to the fact that Au hardly dissociates molecular hydrogen. This fact has been also ascribed to its lack of a partially filled d-band where electrons from the reactant molecules can be received, at least at the low temperatures, where the reaction takes place. From the NP sizes standpoint, it seems that the activation of molecular hydrogen only takes place on small NPs, namely low coordination of gold atoms and high number of low coordination edge and corner sites. As suggested by previous work [23] the hydrogen dissociation on catalysts is the rate-determining step for this hydrogenation. Then for the BD hydrogenation on Au-carbon

catalysts, the highest ability of hydrogen chemisorption/dissociation leads to the highest catalytic activity.

The catalytic properties of gold supported on the different GO_{series} and CNT_{series} surfaces were comparatively evaluated. The samples annealed at 300 ºC were not included due to the absence of gold NPs as confirmed above. BD is hydrogenated to a mixture of 1-butene (B), cis-2-butene (C), trans-2-butene (T) and all butenes can be converted to butane upon further hydrogenation. The catalyst activity and the evolution of the hydrogenation products (selectivity) over the different catalysts are shown in Figures 11 and 13. The conversion was zero in the blank tests with the bare nano-carbon supports. From the BD conversions the specific mass activity of each gold catalyst were estimated.
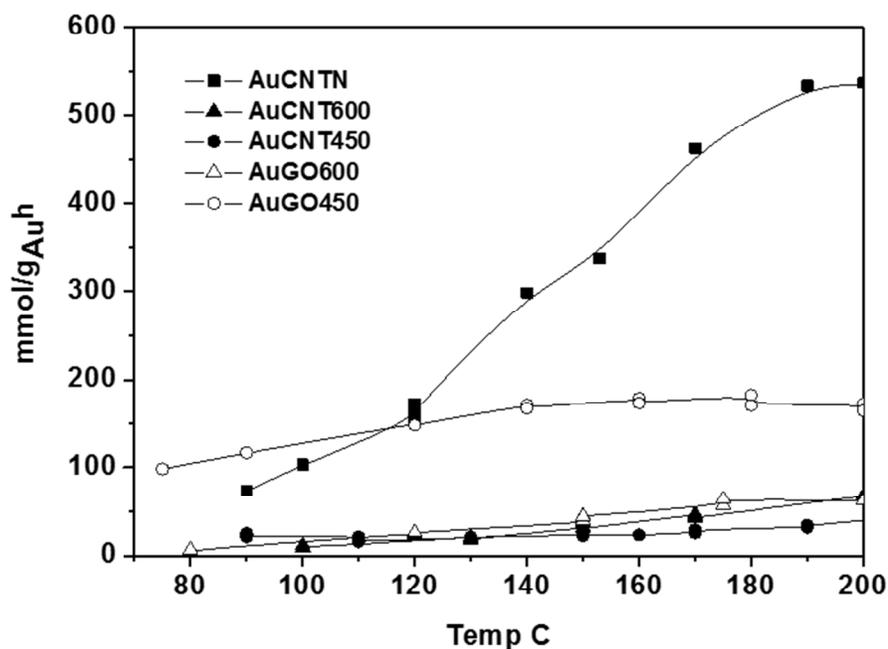

Figure 11. Specific activities of $AuGO_{series}$ and $AuCNT_{series}$ in BD hydrogenation reaction

Figure 11 shows the effect of reaction temperature on BD activities over AuGOs and AuCNTs catalysts. The order of catalytic activity $AuGO_{450}{>}AuCNT_N{>} AuGO_{600} \sim AuCNT_{450} \sim AuCNT_{600}$ was evident in the range of reaction temperatures 90-120 ºC. Between 120-200 ºC the catalytic activity order changed to $AuCNT_N{>} AuGO_{450}{>} AuGO_{600} \sim AuCNT_{450} \sim AuCNT_{600}$ indicating that $AuCNT_N$ possesses the highest catalytic activity at higher temperatures. Even though the mean particle size for $AuCNT_N$ was quite large (12.7 nm), it contained a significant population of

AuNPs<5 nm (40.1%, obtained by TEM), which could explain its higher specific activities at high temperatures. $AuGO_{450}$ and $AuGO_{600}$ exhibited 23.2 % and 14.8 % of NPs below 5 nm respectively. However its lower activity at high temperatures needs further explanation. Although the optimum NPs size for BD hydrogenation is not clear, one can assume that NPs under 5 nm are the active ones. The large sizes of AuNPs below 5 nm are responsible of the poor activity, considering that such Au nanoparticles hardly dissociates the molecular H_2 due to lack of low coordination sites on these gold NPs. Molecular hydrogen does not chemisorb on bulk gold. Dissociative H_2 adsorption/activation is favoured on low coordinated Au (corner and edge) sites that are diminished in number on AuNPs higher than 5 nm, resulting in reduced hydrogenation efficiency. Moreover it has been reported that the reactivity of BD is only slightly structure sensitive to particle size below 5 nm [50-52].

The order of specific activities cannot be directly related neither with the average particle sizes (Table 2) nor with the fraction of smaller Au particles (Table 3). So the order of activity at 100 ºC of reaction temperature: $AuGO_{450}$ >$AuCNT_N$>>others, is reversed when the reaction temperature increase up to 120 ºC, becoming $AuCNT_N$> $AuGO_{450}$ >> others. These findings can be interpreted as consequence of the modification in the apparent energy of activation of the reaction, and thus this principal difference is associated to an effect of the two supports (GO_{450} versus CNT_N). If we remember that the reaction is controlled by the availability of reactive hydrogen species (dissociation/activation of molecular H_2 and the possible migration of adsorbed species between metal and support) we can postulate that $AuGO_{450}$ and particularly $AuCNT_N$ (at high temperature) exhibit an interesting capability for hydrogen spillover. Hydrogen spillover is described as the dissociation of hydrogen molecules over the metal surface, followed by the migration of the H atoms onto the adjacent surface of the support and the diffusion and adsorption of the H atoms on the support. Notice that this capability is not directly related with the amount of nitrogen surface groups exposed in the carbonaceous supports (for instance comparing GO_{450} and GO_{600}), but the key point to explain these spillover differences should be associated with the previously discussed nature of the generated species. Chung et al. [52] postulated that the oxygen functional groups facilitated the diffusion of the surface spillover H atoms rather than providing adsorption sites. Moreover the surface diffusion is enhanced by the continuous network of these oxygen groups, which results in several strong adsorption sites.

Turning again on the CNTs supports, it has been reported that the hydrogen atoms (activated/dissociated on the surface of Au NPs) can spillover through the defects of CNTs [53]

and can be stored at some defect sites. So it is expected that hydrogen storage capacity should vary depending on the number of defects. A. Z. Moshfegh et al. [54] consider that hydrogen molecules are adsorbed on the defect sites by means of physical adsorption and they are transported to the spaces between adjacent carbon layers of the MWCNTs via diffusion of defect sites. Moreover, they are stored on the sp^2 structures and defect sites. Some works have shown that the highest ability of hydrogen chemisorption/dissociation on AuCNT catalyst leads to the highest catalytic activity [23]. Moreover hydrogen uptake is also dependent on temperature and Bus et al. [55] demonstrated an increase in the amount of chemisorbed hydrogen with an increase in the temperature (298 K-373 K). Whether H atoms can spillover/diffuse onto other portions of the gold surface after dissociating on active sites, such as low-coordinated gold sites, interfaces and support is still an open question [56]. TEM observations revealed a greater number of carbon vacancies in the curved graphitic sheets (the existence of five or seven membered rings) and the presence of amorphous carbon on CNT_N (Fig. 9) in comparison with the other samples. Also the XPS results (Fig. 12) showed that the C1s spectra can be decomposed into eight components corresponding to graphitic sp^2 carbon (284.6 eV), or sp^3 carbon (285.1 eV), $Csp^2 - N$ (285.8 eV), carbon in single C-O bonds as ether, alcohol, phenol (286.6 eV), $Csp^3 - N$ (287.9 eV), carbon in carbonyl groups (287.5 eV), carbon in carboxyl or ester groups (289.3 eV) and the $\pi \rightarrow \pi*$ shake-up peak (290.6 eV). In the case of CNT_N , GO_{450} and GO_{600} the C1s envelope width is due to the component assigned to graphitic carbon and a high contribution assigned to defects, unlike in other samples. These defect sites could be located on the interface of the supports and Au NPs can be directly anchored on these sites. In the case of CNTs, BET results indicated that CNT_N exhibits higher surface area and therefore higher number of defects per gram compared with GO samples. This suggests that there are more defects sites on CNT_N and also that the interaction with the support is enhanced when the Au metal particles are smaller (Table 2) explaining the activity order. Then, a trend between the BET surface areas and the activity could be observed.
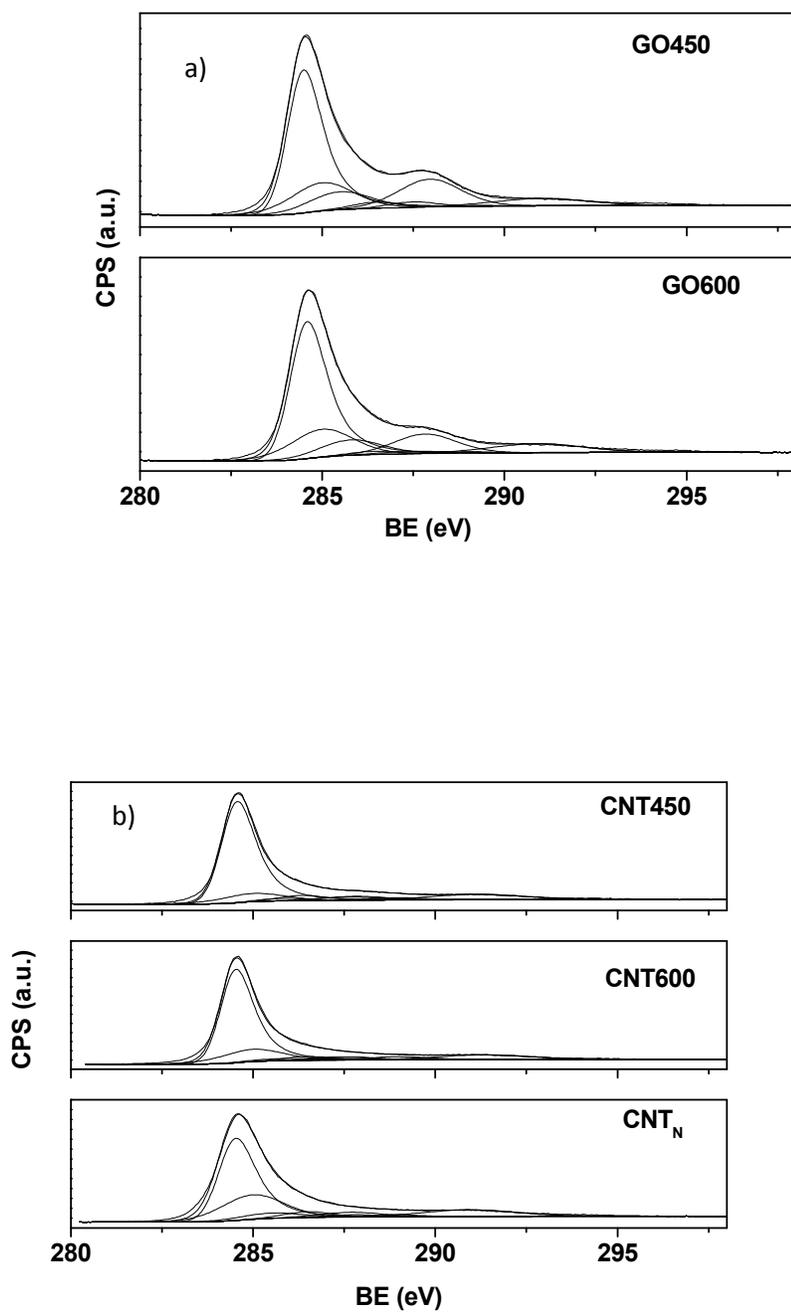
Figure 12. XPS spectra of: a) C 1s GO$_{series}$ and b) C 1s CNT$_{series}$

On the other hand, Zhang et al. [57] have studied the interaction between small molecules and graphene surfaces. They found that the graphene sheets adsorb H_2 molecules when it is doped. However, the added N atoms did not improve the interactions between the N-doped graphene sheets and the hydrogen molecule. Then, we presume that spillover effect should be small over $AuGO_{600}$ in comparison with $AuGO_{450}$, and that the higher activity of the second should be related with the migration of adsorbed species over the surface groups (it should be remembered that $AuGO_{450}$ presents higher proportion of surface groups when compared with $AuGO_{600}$).

In short these results could be interpreted in terms not only of a mechanism in which BD is adsorbed on the gold surface but also as a consequence of the migration of hydrogen species from the support to the metal by a reverse spillover mechanism [58].

Aiming to understand the lower catalytic activities at high temperatures of $AuGO_{600}$ and of $AuGO_{450}$ in the BD hydrogenation and its dependency with the support functional groups; XPS spectra have been carefully inspected. In the case of GO_{450} exhibits amides, amine, pyridinic nitrogen, pyrollic nitrogen and quaternary nitrogen, meanwhile GO_{600} exhibits an increase in the quaternary nitrogen and a decrease in the pyrrolic/amide nitrogen groups. However only the higher surface area of CNT_N and therefore higher number of defects per gram could explain its catalytic activity at high temperature. Moreover, with temperature the hydrogen uptake (chemisorbed H_2) by supported gold increases being higher on $AuCNT_N$. In the case of $AuGO_{450}$, the chemisorbed H_2 seems to depend on the surface groups and not on the temperature.

In the case of $AuCNT_{450}$ and $AuCNT_{600}$, the higher proportion of large size Au particles can justify the low catalytic activities achieved in these cases. However the order of catalytic activity is similar to AuGO600 (smaller particle size) where chemisorbed H_2 appears to be much lower.

The evolution of the selectivities to butenes with the reaction temperature also depends on the studied catalyst (Fig. 13). 1-Butene was the main product for $AuGO_{600}$ and $AuCNT_{600}$. The percentages in the different butenes varied as follows: 1-butene>trans-2-butene>cis-2-butene. Its proportion did not significantly change with the temperature indicating no isomerisation. Also over $AuCNT_N$ 1-butene is the main product, and only at reaction temperatures higher than 170 ºC its selectivity becomes equal to that towards trans-2-butene.

In the case of $AuCNT_{450}$ initially1-butene was the main product but its percentage varies with the temperature. Here, the proportions change with the temperature indicating a slight isomerisation between 1-butene and 2-butenes [59]. Okumura et al. reported experiments over Au/Al_2O_3 [60] where 1-butene isomerises to 2-butenes (especially to trans-2-butene which is the most stable

butene) when the reaction temperature increase. Also these authors correlated this high selectivity to 1-butene with the high Pauling electronegativity of metallic Au. Finally, $AuGO_{450}$ possesses the highest catalytic activity at low temperature and the percentages of the different butenes vary as follows: trans-2-butene>1-butene>butane>cis-2-butene. This proportion does not significantly change with the reaction temperature indicating lack of isomerisation. In general, the trans/cis-2-butene ratio slightly decreases with increasing temperature.

Yang et al. [61] proposed that on gold NPs smaller than 5 nm, the formation of the cis-2-butene might be favoured compared with that of trans-2-butene due to the preferential adsorption of cis-1,3-butadiene isomer on the low coordination sites of the edges or corners. It is well known that particle size decreasing leads to a diminution in the average coordination number of metal atoms and to an increasing in the number of the low-coordination edge and corner sites. They also observed a stronger orbital interaction between cis-1,3-butadiene and low-coordination gold atoms. Thus, the adsorption of the cis isomer on small AuNPs (<5nm) is thermodynamically favourable and the trans-to-cis transformation of BD is kinetically facile. Moreover the cis/trans-2-butene ratio decreases with increasing AuNPs size.
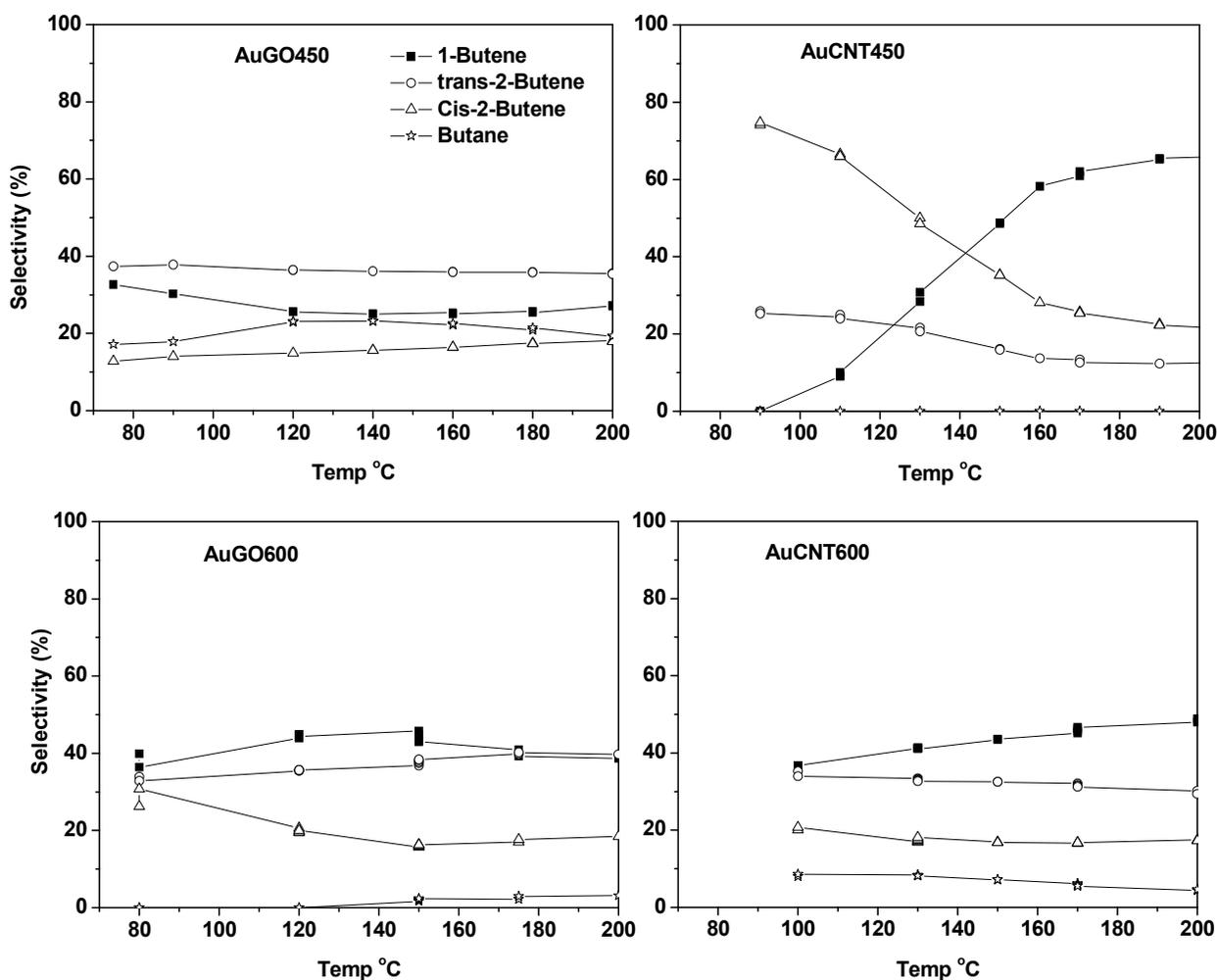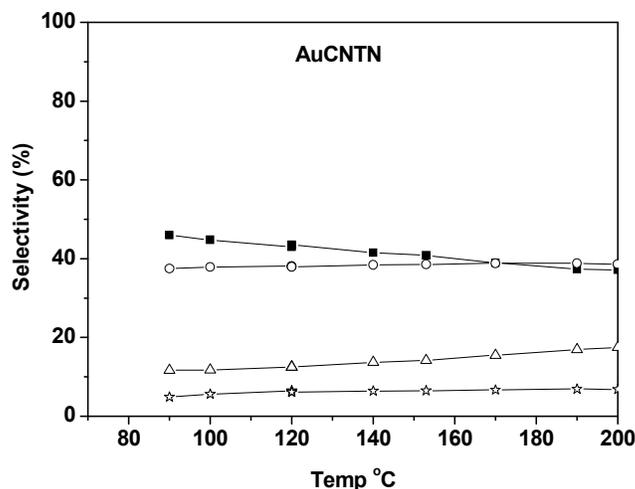
Figure 14. Evolution of the selectivity (%) to 1-butene, trans-2-butene, cis-2-butene and butane.

In the present study, the samples exhibited a broad distribution of particle sizes. The reasons for the differences of selectivities may result from the difference in particle size distributions, proving a correlation between the selectivities and the Au NPs size [62]. Thus, in catalysts with distribution including mainly larger NPs there are different planes and lower proportion of low-coordinated surface sites exits. This different situation gives place to different adsorption modes of the reactant onto the surface, and these would govern the selectivity suggesting that control of the intramolecular selectivity is structure-sensitive. On the other hand, the evolution of selectivities when increasing the reaction temperatures cannot be explained as due to a sintering effect of the Au metallic particles, both because the catalysts are reduced at higher temperature than those of the reaction, and because when the reaction is studied at decreasing temperatures the selectivity values are restored. In short these modifications of selectivity could be associated to deposits of partially unsaturated hydrocarbons that can block the Au surface sites.

Conclusions

This systematic study of the N-doped carbon (GO_{series} and CNT_{series}) samples, prepared by thermal annealing with urea, has shown that the basicity of the support permits the precipitation of the Au precursor solution over the entire surface. Therefore, urea treatments can be used to change the carbon properties and they can provide a suitable surface for attaching the Au NPs. If the annealing treatment is not performed at high temperatures, more than 300ºC, the resulting support material is too acidic, and Au NPs are not retained over these surfaces.

The formation of cyanuric acid is reported at the early stages of the annealing process. Below 450ºC thermal treatment, N-amide linkages with the oxygen functional groups of the graphene sheets, and pyridinic, pyrrolic and quaternary nitrogen are found. Finally at higher temperature (600 ºC) there is an increase in the quaternary nitrogen and a decrease in the pyrrolic/amide nitrogen groups. Additionally, we have shown that these nano-carbon materials doped with nitrogen are a promising support for gold catalysts. These catalysts exhibited high catalytic activity and high stability for the 1,3-BD hydrogenation. Factors such as hydrogen chemisorption, hydrogen spillover or migration of adsorbed species between metal-support, as well as enrichment of reactant over Au NPs (strong adsorbed species) have been revealed to have impacts on the catalytic performance, specific activities and selectivity values. Finally, it has been verified that the selectivity is highly size dependent.

References

[1] Su D S, Perathoner S, Centi G,Nanocarbons for the development of advanced catalysts, *Chem Rev*, 2013, **113**, 5782-5816.
[2] Serp P, Carbon nanotubes and nanofibers in catalysis. In: P. Serp& J.L. Figueiredo editors. Carbon materials for catalysis. J. Wiley & Sons, Hoboken (NJ); 2009 p. 309-372
[3] Serp P, Castillejos E, Catalysis in Carbon Nanotubes, *Chemcatchem,* 2010, **2**, 41-47.

[4] Castillejos E, Debouttière P J, Roiban L, Solhy A, Martinez V, Kihn Y, Ersen O, Philippot K, Chaudret B, Serp P, An efficient strategy to drive nanoparticles into carbon nanotubes and the remarkable effect of confinement on their catalytic performance, *Angew Chem Int Ed,* 2009, **48**, 2529-2533.

[5] Dongil A B, Bachiller-Baeza B, Guerrero-Ruiz A, Rodríguez-Ramos I, Chemoselective hydrogenation of cinnamaldehyde: A comparison of the immobilization of Ru–phosphine complex on graphite oxide and on graphitic surfaces, *J Catal*, 2011, **282**, 299-309.

[6] Stankovich S, Dikin D A, Piner R D, Kohlhaas K A, KleinhammesA, Jia Y, Wu Y, Nguyen S T, Ruoff R S, Synthesis of graphene-based nanosheets via chemical reduction of exfoliated graphite oxide, *Carbon*, 2007, **45**, 1558-1565.

[7] Dreye rD R, Park S, Bielawski C W, Ruoff R S, The chemistry of graphene oxide, *Chem Soc Rev*, 2010, **39**, 228-240.

[8] McAllister M J, Li J-L, Adamson D H, Schniepp H C, Abdala A A, Liu J, Herrera-Alonso M, Milius D L, Car R, Prud'homme R K, Aksay I A, Single sheet functionalized graphene by oxidation and thermal expansion of graphite, *Chem Mater*, 2007, **19**, 4396-4404.

[9] Machado B F, Serp P, Graphene-based materials for catalysis, Catalsci&techn, 2012, **2**, 54-75.

[10] Figueiredo J L, Pereira M F R, Freitas M M A, Órfão J J, Modification of the surface chemistry of activated carbons, *Carbon, 1999,* **37**, 1379.

[11] Castillejos E, Chico R, Bacsa R, Coco S, Espinet P, Perez-Cadenas M, Guerrero-Ruiz A, Rodríguez-Ramos I, Serp P, Selective deposition of gold nanoparticles on or in side carbon nanotubes and their catalytic activity for preferential oxidation of CO, *Eur J Inorg Chem,* 2010, **32**, 5096-5102.

[12] Haruta M, Yamada N, Kobayashi T, Iijima S, Gold catalysts prepared by coprecipitation for low-temperature oxidation of hydrogen and of carbon monoxide, *J Catal*, 1989, **115**, 301.

[13] Haruta M, Tsubota S, Kobayashi T, Kageyama H, Genet M J, Delmon B, Low-Temperature oxidation of CO over gold supported on TiO2, α-Fe2O3, and Co3O4, *J Catal*, 1993, **144**, 175-192.

[14] Haruta M, Catalysis: Gold rush, Nature 2005, **437**, 1098-1099.

[15] Castillejos E, Bacsa R, Guerrero-Ruiz A, Rodríguez-Ramos I, Datas L, Serp P, Catalytic activity of gold supported on ZnO tetrapods for the preferential oxidation of carbon monoxide under hydrogen rich conditions, *Nanoscale*, 2011, **3**, 929-932.

[16] Corma A, Serna P, Chemoselective hydrogenation of nitro compounds with supported gold catalysts, *Science,* 2006, **313**, 332-334.

[17] Castillejos E, Gallegos-Suarez E, Bachiller-Baeza B, Bacsa R, Serp P, Guerrero-Ruiz A, Rodríguez-Ramos I, Deposition of gold nanoparticles on ZnO and their catalytic activity for hydrogenation applications, *Catal Comm*, 2012, **22**, 79-82.

[18] Nishina N, YamamotoY, Gold-catalyzed intermolecular hydroamination of allenes with arylamines and resulting high chirality transfer, *Angew Chem*, 2006, **118**, 3392-3395.

[19] Corma A, Concepción P, Dominguez I, Fornés V, Sabater M J, Gold supported on a biopolymer (chitosan) catalyzes the region selective hydroamination of alkynes, *J Catal,* 2007, **251**, 39-47.

[20] Stephen A, Hashmi K, Frost T M, Bats J W, Highly selective gold-catalyzed arene synthesis, *J Am Chem Soc,* 2000, **122**, 11553-11554.

[21] González-Arellano C, Abad A, Corma A, Garcia H, Iglesias M, Sanchez F, Catalysis by gold(I) and gold (III): a parallelism between homo-and heterogeneous catalysts for copper-free sonogashira cross-coupling reactions, *Angew Chem Int Ed,* 2007, **46**, 1536-1538.

[22] Haruta M, When gold is not noble: catalysis by nanoparticles, *Chem Rec*, 2003, **3**, 75-87.

[23] Zhang X, Guo Y C, Zhang Z C, Gao J S, Xu C M,High performance of carbon nanotubes confining gold nanoparticles for selective hydrogenation of 1,3-butadiene and cinnamaldehyde, *J Catal*, 2012, **292**, 213-226.

[24] Singh R, Premkumar T, Shin J-Y, Geckeler K E, Carbon nanotube and gold-based materials: a symbiosis, *Chem Eur J,* 2010, **16**, 1728-1743.

[25] Matsuda Y, Deng W Q, Goddard W A, Contact resistance properties between nanotubes and various metals from quantum mechanics, *J Phys Chem C*, 2007, **111**, 11113-11116.

[26] Brodie B C, On the atomic weight of graphite, *Philos Trans Roy Soc Lond*, 1859, **149**, 249-259.

[27] Mou Z, Chen X, Du Y, Wang X, Yang P, Wang S, Forming mechanism of nitrogen doped graphene prepared by thermal solid-state reaction of graphite oxide and urea, *Appl Surf Sci*, 2011, **258**, 1704-1710

[28] Castillejos-Lopez E, Nevskaia D M, Munoz V, Rodríguez-Ramos I, Guerrero-Ruiz A, On the interactions of phenol, aniline and p-nitrophenol on activated carbon surfaces as detected by TPD, *Carbon*, 2008, **46**, 870-875.

[29] Garcia-Garcia F R, Alvarez-Rodríguez J, Rodríguez-Ramos I, Guerrero-Ruiz A, The use of carbon nanotubes with and without nitrogen doping as support for ruthenium catalysts in the ammonia decomposition reaction, *Carbon,* 2010, **48**, 267-276.

[30] Asedegbega-Nieto E, Perez-Cadenas M, Morales M V, Bachiller-Baeza B, Gallegos-Suarez E, Rodríguez-Ramos I, Guerrero-Ruiz A, High nitrogen doped graphenes and their applicability as basic catalysts, *Diam Relat Mater*, 2014, **44**, 26-32.

[31] Mircescu N E, Oltean M, ChisV, Leopold N, FTIR, FT-Raman, SERS and DFT study on melamine, *Vibrational Spectroscopy,* 2012, **62**, 165-171.

[32] Widerski G S, Wojtulewski S, Kalinowska M, wisłocka R S, Lewandowski W, Effect of alkali metal ions on the pyrrole and pyridine π-electron systems in pyrrole-2-carboxylate and pyridine-2-carboxylate molecules: FT-IR, FT-Raman, NMR and theoretical studies, *J Mol Struct*, 2011, **993**, 448-458.

[33] Stankovich S, Piner R D, Nguyen S T, Ruoff R S, Synthesis and exfoliation of isocyanate-treated graphene oxide nanoplatelets, *Carbon,* 2006, **44**, 3342-3347.

[34] Yu H, Tao Y, Chen D, Wang Y, Liu Z, Pan Y, Huang L, Peng D, Dai M, Liu Z, Yuan Z, *Anal Chim Acta*, 2010, **682**,48-58.

[35] Isbasara C, Hacaloglu J, Investigation of thermal degradation characteristics of polyamide-6 containing melamine or melamine cyanurate via direct pyrolysis mass spectrometry, *J Anal Appl Pyrol,* 2012, **98**, 221-230.

[36] Hon P Y T, Chu P W S, Cheng C-H, Lee T C L, Chan P-k, Cheung S T C, Wong Y-C, Development of melamine certified reference material in milk using two different isotope dilution mass spectrometry techniques, *J Chrom A,* 2011, **1218**, 6907-6913.

[37] Gridelet E, Locht R, Lorquet A J, Lorquet J C, Leyh B, How ergodic is the fragmentation of the pyridine cation?: A maximum entropy analysis, *Int J Mass Spectrom*, 2003, **228**, 389-402

[38] Arrigo R, Hävecker M, Schlögl R, Su D S, Dynamic surface rearrangement and thermal stability of nitrogen functional groups on carbon, *ChemCommun*, 2008, 4891.

[39] Lai L, Chen L, Zhan D, Sun L, Liu J, Lim S H, Poh C K, Shen Z, Lin J, One-step synthesis of NH2-graphene from in situ graphene-oxide reduction and its improved electrochemical properties *Carbon*, 2011, **49**, 3250-3257.

[40] Tang X-Z, Li W, Yu Z-Z, Rafiee M A, Rafiee J, Yavari F, Koratkar N, Enhanced thermal stability in graphene oxide covalently functionalized with 2-amino-4,6-didodecylamino-1,3,5-triazine, *Carbon*, 2011, **49**, 1258-1265.

[41] Yang G, Han H, Du C, Luo Z, Wang Y, Facile synthesis of melamine-based porous polymer networks and their application for removal of aqueous mercury ions, *Polymer* 2010, **51**, 6193-6202.

[42] Jansen R J J, Van Bekum H, Hydrophobically end-capped polyethylene-oxide urethanes: 2. Modelling their association in water, *Carbon*, 1995, **33**, 1021-1025.

[43] Geng D, Yang S, Zhang Y, Yang J, Liu J, Li R, ShamT-K, SunX, YeS, KnightsS, Nitrogen doping effects on the structure of graphene, *Appl Surf Sci*, 2011, **257**, 9193-9198.

[44] Li Y, Wang J, Li X, Geng D, Banis M N, Li R, Sun X, Nitrogen-doped graphene nanosheets as cathode materials with excellent electrocatalytic activity for high capacity lithium-oxygen batteries *Electrochem Comm*. 2012, **18**, 12-15.

[45] Zhang C, Hao R, Liao H, Hou Y, Synthesis of amino-functionalized graphene as metal-free catalyst and exploration of the roles of various nitrogen states in oxygen reduction reaction, *Nano Energy*, 2013, **2**, 88-97.

[46] Prati L, Villa A, Lupini A R, Veith G M, Gold on carbon: one billion catalysts under a single label, Phys *Chem Chem Phys*, 2012, 14, 2969-2978.

[47] Peters S, Peredkov S, Neeb M, Eberhardt W, Al-Hada M, Size-dependent XPS spectra of small supported Au-clusters, *Surf Sci*, 2013, **608**, 129-134.

[48] MikhlinY L, Romanchenko A S, Gold deposition on pyrite and the common sulfide minerals: An STM/STS and SR-XPS study of surface reactions and Au nanoparticles, *Geo Cosmo chim Ac,* 2007, **71**, 5985-6001.

[49] Souza K R, de Lima A F F, De Sousa F F, Appel L G*,* Preparing Au/ZnO by precipitation–deposition technique, *Appl Catal A: Gen*, 2008, **340**, 133-139.

[50] Dommele S V, De Jong K P, Bitter J H, Nitrogen-containing carbon nanotubes as solid base catalysts *Chemcom*, 2006, **46**, 4859-4861.

[51] Zhang Y, Cui X, Shi F, Deng Y, Nano-gold catalysis in fine chemical synthesis, *Chem Rev*, 2012, **112**, 2467-2505.

[52] Chung T-Y, Tsao C-S, Tseng H-P, Chen C-H, Yu M-S, Effects of oxygen functional groups on the enhancement of the hydrogen spillover of Pd-doped activated carbon, *J Collo Inter Sci*, 2015, 441, 98-105.

[53] Yoo E, Gao L, Komatsu T, Yagai N, Arai K, Yamazaki T, Matsuishi K, Matsumoto T, Nakamura J*,* Atomic hydrogen storage in carbon nanotubes promoted by metal catalysts, *J Phys Chem B,* 2004, **108** (49), 18903-18907.

[54] Reyhani A, Mortazavi S Z, Mirershadi S, Golikand A N, Moshfegh A Z, H2 adsorption mechanism in Mg modified multi-walled carbon nanotubes for hydrogen storage, *Int J Hydrog Ener*, 2012, **37**, 1919-1926.

[55] Bus E, Miller J T, van Bokhoven J A, Hydrogen chemisorption on Al2O3-supported gold catalysts, *J Phys Chem. B* 2005, **109** ,14581-14587.

[56] Pan M, Brush A J, Pozun Z D, Ham H C, Yu W-Y, Henkelman G, Hwang G S, Mullins C B, Model studies of heterogeneous catalytic hydrogenation reactions with gold, *Chem Soc Rev,* 2013, **42**, 5002-5013.

[57] Zhang H-P, Luo X-G, Lin X-Y, Lu X, Leng Y, Density functional theory calculations of hydrogen adsorption on Ti, Zn, Zr, Al, and N-doped and intrinsic graphene sheets, *J Hydrog Ener,* 2013, **38**, 14269-14275.

[58] Buchanan D A, Webb G, Catalysis by group IB metals. Part 1. Reaction of buta-1,3-diene with hydrogen and with deuterium catalysed by alumina-supported gold, *J Chem Soc Farad Trans*, 1, 1975, **71**, 134-144.

[59] Hugon A, Delannoy L, Luis C, Supported gold catalysts for selective hydrogenation of 1,3-butadiene in the presence of an excess of alkenes, *Gold Bull*, 2008, **41**, 127-138

[60] Okumura M, Akita T, Haruta M, Hydrogenation of 1,3-butadiene and of crotonaldehyde over highly dispersed Au catalysts, *Catal Today,* 2002, **74**, 265-269.

[61] Yang X-F, Wang A-Q, Wang Y-L, Zhang T, Li J, Unusual selectivity of gold catalysts for hydrogenation of 1,3-butadiene toward cis-2-butene: A joint experimental and theoretical investigation, *J Phys Chem C*, 2010, **114**, 3131-3139.

[62] El Kolli N, Delannoy L, Louis C, Bimetallic Au–Pd catalysts for selective hydrogenation of butadiene: Influence of the preparation method on catalytic properties, *J Catal*, 2013, **297**, 79-92.